

Supplement of

High frequency of new particle formation events driven by summer monsoon in the central Tibetan Plateau, China

Lizi Tang¹, Min Hu^{*1,2}, Dongjie Shang¹, Xin Fang¹, Jianjiong Mao², Wanyun Xu³, Jiacheng Zhou⁴, Weixiong Zhao⁴, Yaru Wang¹, Chong Zhang¹, Yingjie Zhang⁵, Jianlin Hu², Limin Zeng^{1,2}, Chunxiang Ye¹, Song Guo^{1,2}, Zhijun Wu^{1,2}

¹State Key Joint Laboratory of Environmental Simulation and Pollution Control, International Joint Laboratory for Regional Pollution Control, Ministry of Education (IJRC), College of Environmental Sciences and Engineering, Peking University, Beijing 100871, China

²Collaborative Innovation Center of Atmospheric Environment and Equipment Technology, Jiangsu Key Laboratory of Atmospheric Environment Monitoring and Pollution Control. Nanjing University of Information Science & Technology, Nanjing 210044, China

³State Key Laboratory of Severe Weather & Key Laboratory for Atmospheric Chemistry of CMA, Institute of Atmospheric Composition, Chinese Academy of Meteorological Sciences, Beijing, 100081, China

⁴Laboratory of Atmospheric Physico-Chemistry, Anhui Institute of Optics and Fine Mechanisms, HFIPS, Chinese Academy of Science, Hefei 230031, Anhui, China

⁵School of Ecology and Nature Conservation, Beijing Forestry University, Beijing 100083, China

Correspondence to: Min Hu (minhu@pku.edu.cn).

List of the supporting information:

Text S1. Details about model simulations

Figure S1. WRF/CMAQ modeling domain

Figure S2. Comparison of simulated and observed wind direction and wind speed

Figure S3. Comparison of simulated and observed PM and O₃

Figure S4. Comparison in frequency distributions of temperature, RH, H₂O and WS in pre-monsoon and monsoon seasons

Figure S5. Wind rose plots in pre-monsoon and monsoon seasons

Figure S6. The frequencies of the 48 h back trajectories of air masses in pre-monsoon and monsoon seasons

Figure S7. Comparison in frequency distributions of PM_{0.8}, BC, O₃ and CO in pre-monsoon and monsoon seasons

Figure S8. Model spatial distribution of SO₂ in non-event days, NPF-pre days and NPF-monsoon days

Figure S9. Model spatial distribution of wind in non-event days, NPF-pre days and NPF-monsoon days

Figure S10. Determination of the aerosol production in 17 June, 2019

Text S1 Model simulation

Model Configurations

The meteorological conditions were simulated using the Weather Research and Forecasting (WRF) (version 4.2.1) model with the FNL reanalysis dataset. The 6 h FNL data were obtained from the U.S. National Centre for Atmospheric Research (NCAR), with a spatial resolution of $1.0^\circ \times 1.0^\circ$ (<http://rda.ucar.edu/datasets/ds083.2/>, last accessed on 28 April 2022). The physical parameterizations used in this study are the Thompson microphysical process, RRTMG longwave/shortwave radiation scheme; Noah land-surface scheme; MYJ boundary layer scheme; and modified Tiedtke cumulus parameterization scheme. The detailed configuration settings could be found in the works of Hu et al. (2016), Mao et al. (2022), Wang et al. (2021).

The Community Multiscale Air Quality version 5.3.2 (CMAQv5.3.2) model, being one of the three-dimensional chemical transport models (CTMs) (Appel et al., 2021), configured with the gas-phase mechanism of SAPRC07tic and the aerosol module of AERO6i, was employed in this study to simulate the air quality over Tibet from 24 April to 24 May and 13 June to 27 June in 2019, which contains the observation period. Air quality simulations were performed with a horizontal resolution of 12 km. The corresponding domain covered Tibet and the surrounding countries and regions with 166×166 grids (Fig. S1), with the 18 layers in vertical resolution. The initial and boundary conditions were provided by the default profiles. The simulated results of the first two days were not included in the model analysis, which served as a spin-up and reduced the effects of the initial conditions on the simulated results.

Emission Inventory

The Multi-resolution Emission Inventory for China version 1.3 (MEICv1.3) (<http://www.meicmodel.org>) and Regional Emission inventory in ASia (REASv3.2) (<https://www.nies.go.jp/REAS/>) were used to provide the anthropogenic emissions. MEIC served as the anthropogenic emissions from China, while REAS served as the anthropogenic emissions from neighboring countries and regions. The MEICv1.3 emissions of the year 2019 were used. For REAS, since no emission inventory was released for the years after 2015, we used the emission inventory in the year 2015 for 2019. Although emission inventories are usually released 3 years behind, we acknowledge that this may cause additional uncertainties in the simulation. Biogenic emissions were generated using the Model for Emissions of Gases and Aerosols from Nature (MEGANv2.1) (Guenther et al., 2012) for the whole simulation period. The open biomass burning emissions were processed using the Fire Inventory for NCAR (FINN) during the entire study period (Wiedinmyer et al., 2011).

Model Evaluation

Previous studies have investigated the impacts of meteorological conditions on the formation, transportation, and dissipation of air pollutants (Hu et al., 2016; Hua et al., 2021; Mao et al., 2022; Sulaymon et al., 2021b; Sulaymon et al., 2021a). Therefore, the evaluation of the WRF model performance was carried out before the usage of its meteorological fields

in the CMAQ simulations. The evaluation of the WRF model was achieved by comparing the predicted wind speed (WS, m/s) and wind direction (WD, °) at 10 m above the surface to the observed values. Fig. S2 showed that WS was well simulated both in pre-monsoon and monsoon seasons. WD was well simulated in pre-monsoon season, and there seems to be some deviation in the simulation of north wind in monsoon season. The main reason about the deviation in WD may be due to the poor terrain and complicated weather conditions. Nevertheless, both simulations and measurements showed more frequent southerly winds during monsoon season.

Fig. S3 showed the comparison of simulated daily mean concentration about PM and O₃ in observation site, which were simulated by CMAQ. PM was simulated well during the whole observation period. O₃ was underpredicted obviously, although its trend can be simulated, which may due to the uncertainty of the emission inventory. Above all, we think WRF/CMAQ can simulate pollutants transmission phenomenon in Tibet.

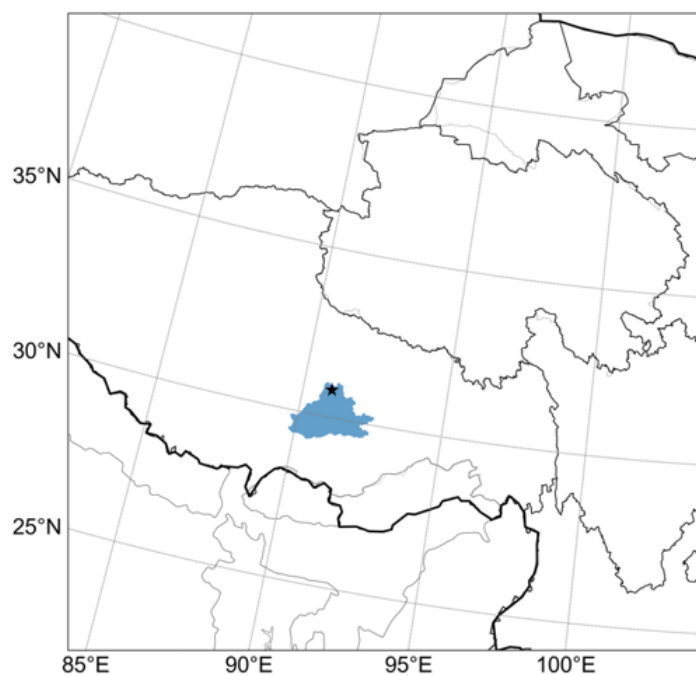


Figure S1. WRF/CMAQ modeling domain

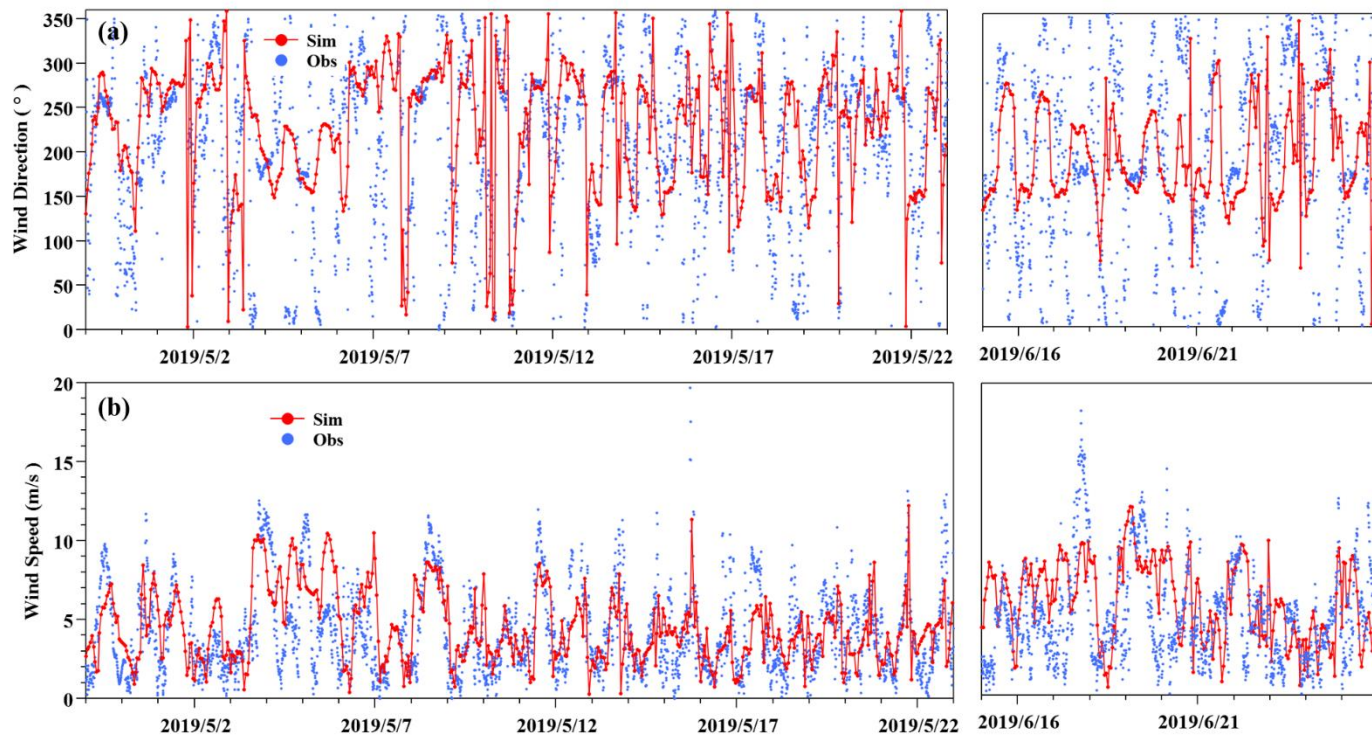


Figure S2. Comparison of simulated (in red dot-line) and observed (in blue dot) wind direction (WD, °) and wind speed (WS, m/s). Observed is 10 minutes mean data. Simulated is hourly mean data.

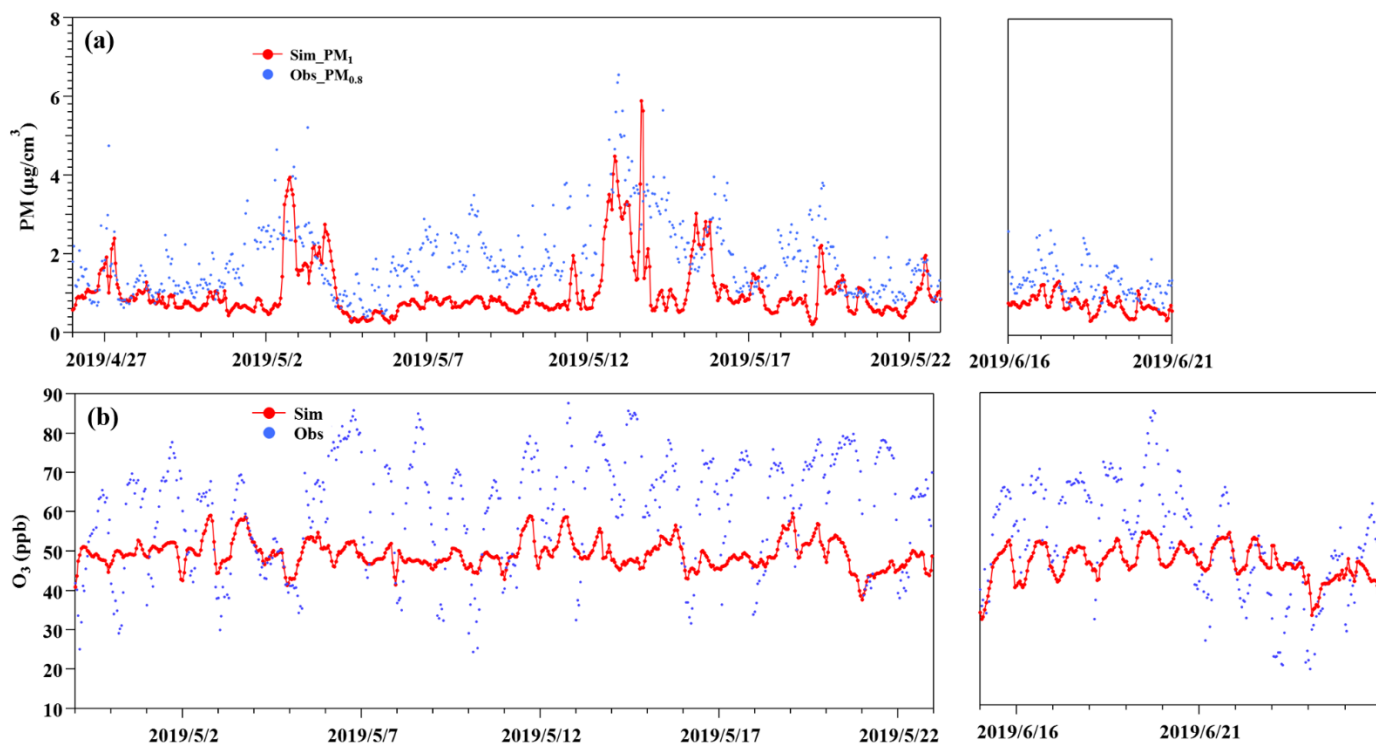


Figure S3. Comparison of simulated (in red dot-line) and observed (in blue dot) PM ($\mu\text{g}/\text{m}^3$) and O_3 (ppb). PM and O_3 both are hourly mean concentration.

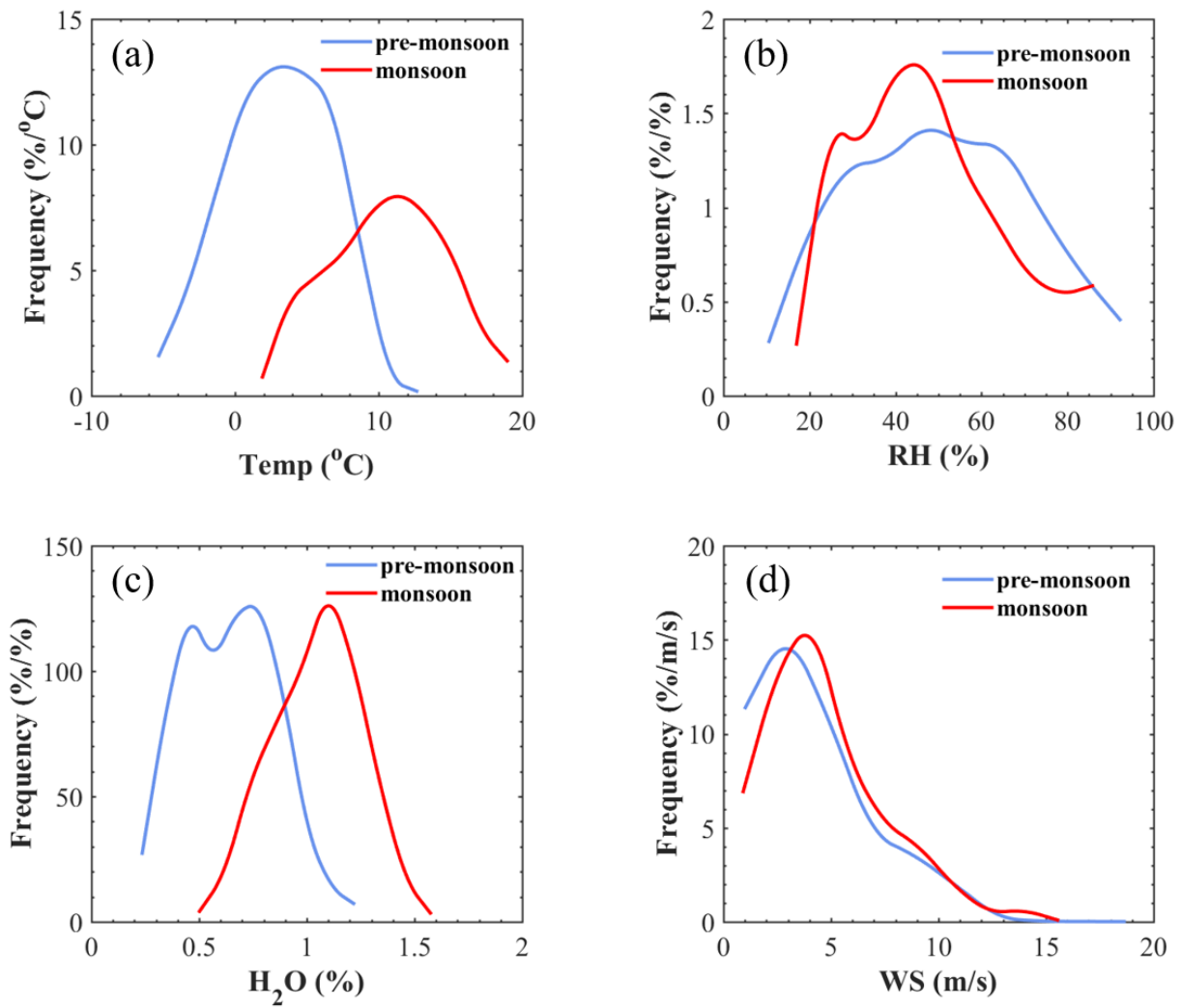


Figure S4. Comparison in frequency distributions of (a) temperature, (b) RH, (c) H₂O and (d) WS at Nam Co station in pre-monsoon and monsoon seasons.

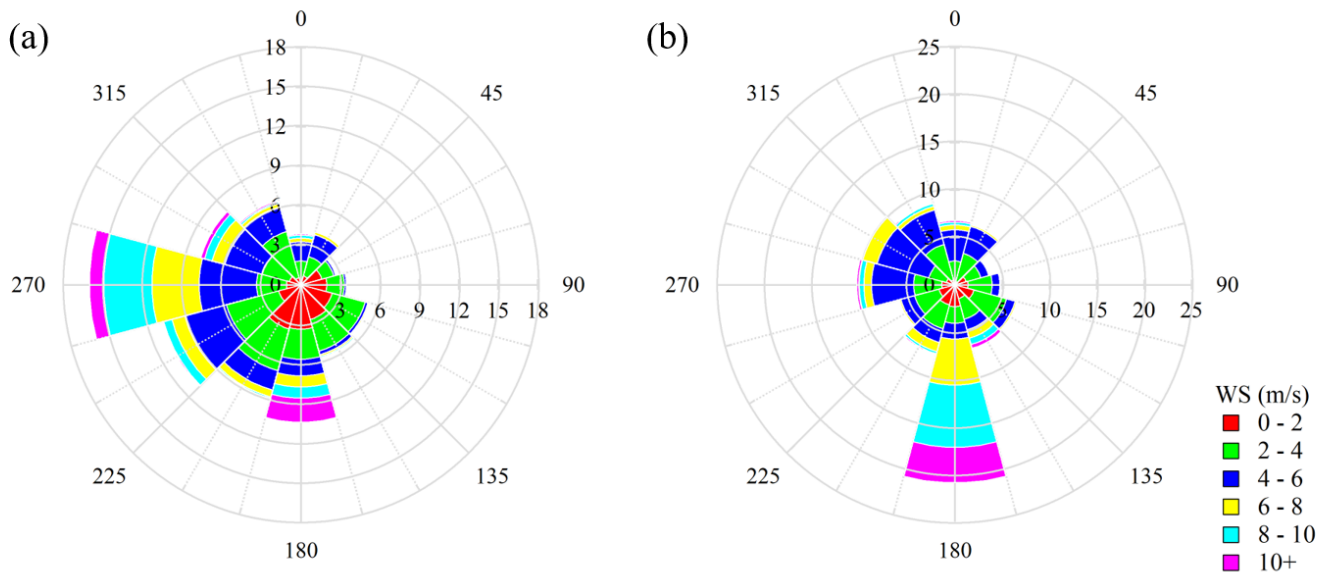


Figure S5. Wind rose plots in (a) pre-monsoon and (b) monsoon seasons. The length of each spoke on the circle represents the probability of wind coming from a particular direction at a certain range of wind speed.

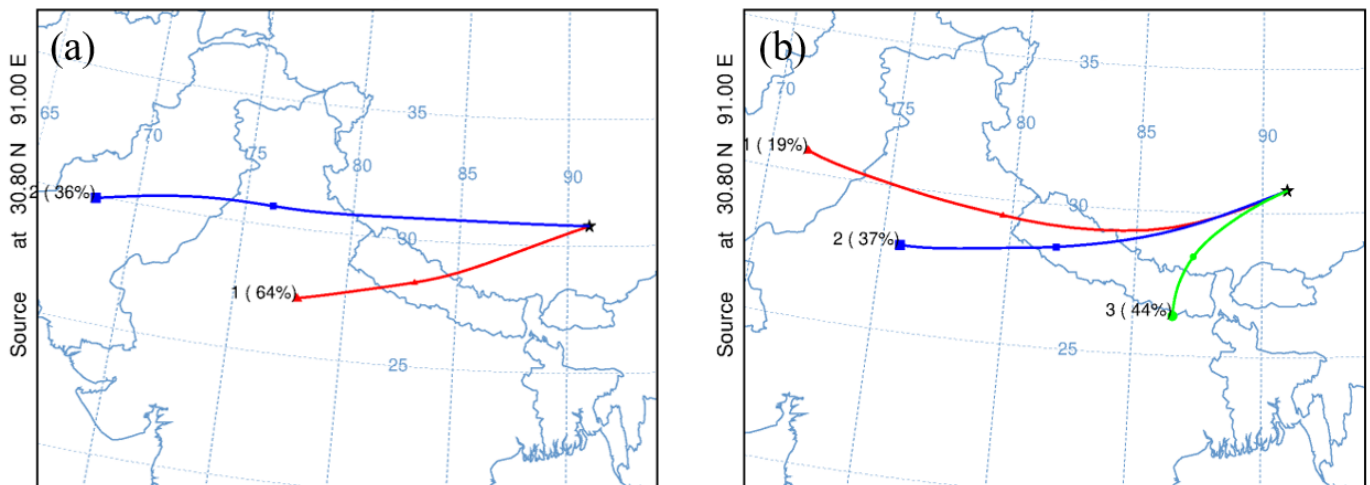


Figure S6. The frequencies of the 48 h back trajectories of air masses arriving at Nam Co station from different directions during (a) pre-monsoon and (b) monsoon seasons.

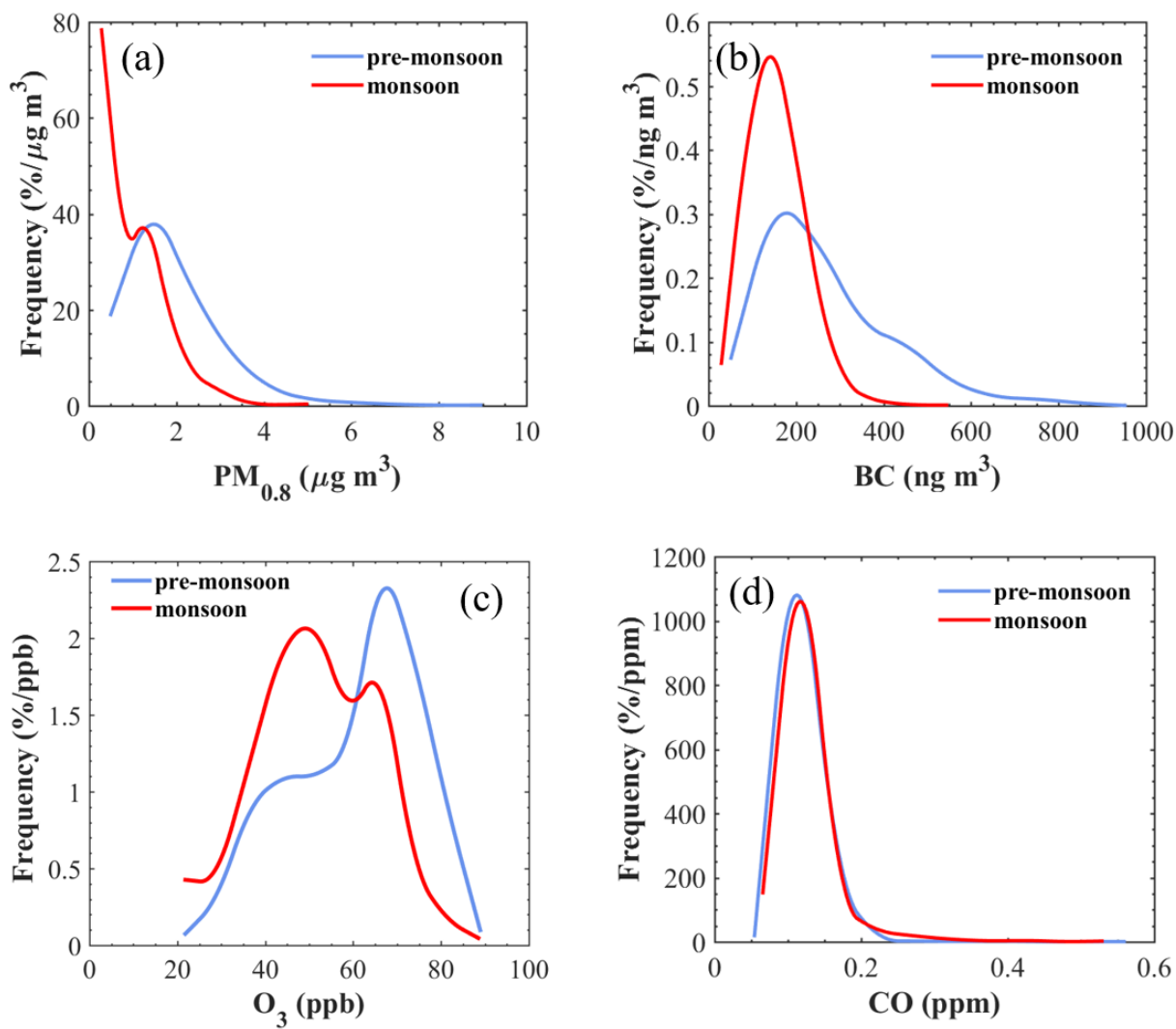


Figure S7. Comparison in frequency distributions of (a) PM_{0.8}, (b) BC, (c) O₃ and (d) CO at Nam Co station in pre-monsoon and monsoon seasons.

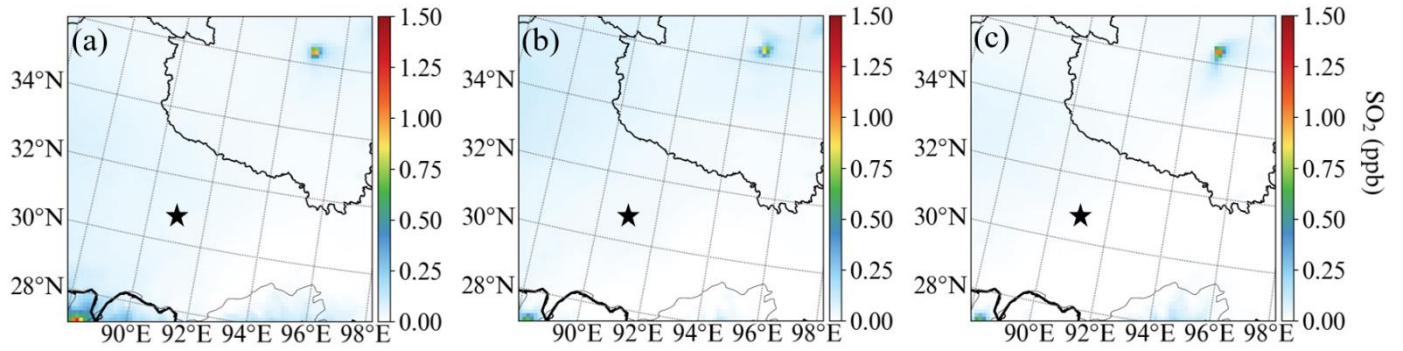


Figure S8. Model spatial distribution of SO₂ in (a) non-event days, (b) NPF-pre days, and (c) NPF-monsoon days. The star is Nam Co station.

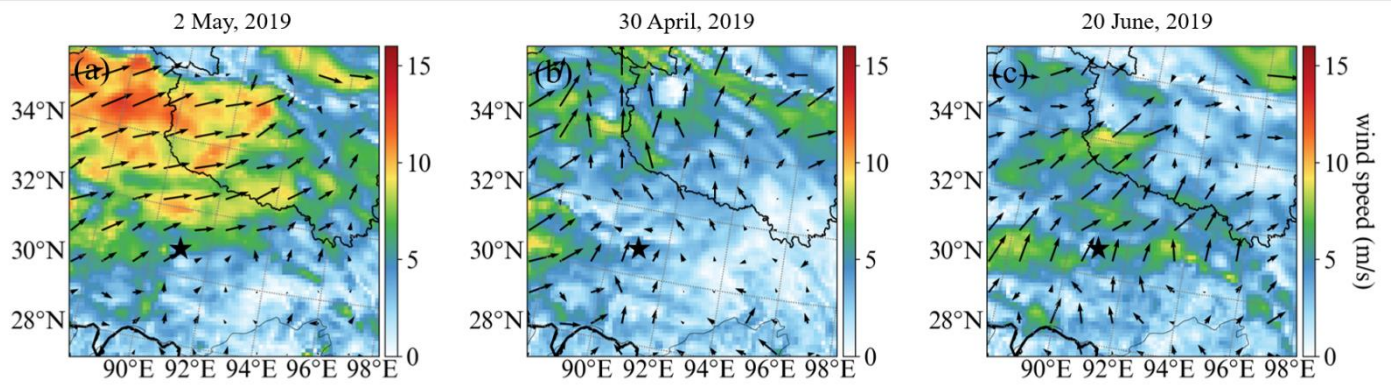


Figure S9. Model spatial distribution of wind at 12:00 in (a) 2 May, 2019 (non-event day), (b) 30 April, 2019 (NPF-pre day), and (c) 20 June, 2019 (NPF-monsoon day), The star is Nam Co station.

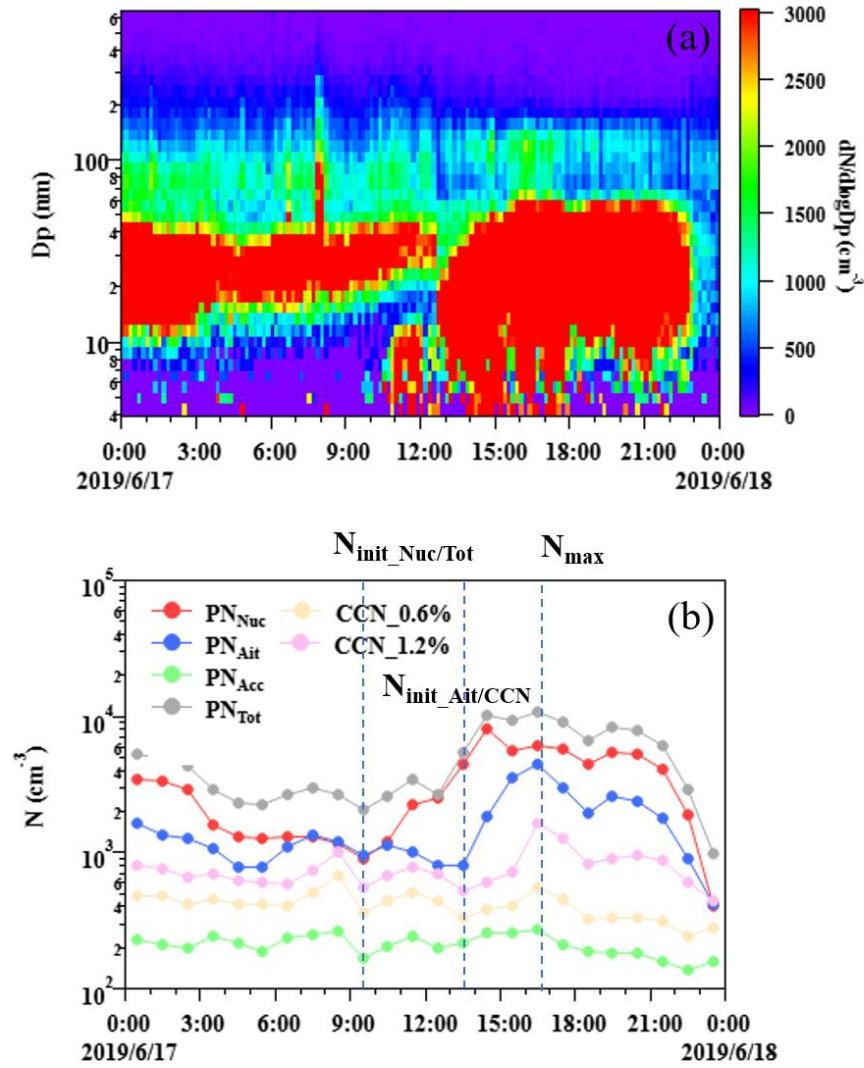


Figure S10. Determination of the aerosol production in 17 June, 2019. Time series of (a) PNSD, and (b) the number concentrations of Nucleation-mode particles (PN_{Nuc}), Aitken-mode particles (PN_{Ait}), Accumulation-mode particles (PN_{Acc}), the total particles (PN_{Tot}), CCN at S_c of 0.6% ($\text{CCN}_{0.6\%}$) and 1.2% ($\text{CCN}_{1.2\%}$) in 17 June, 2019. N_{init} and N_{max} denote, for each mode, the amount from which aerosol production are calculated.

References:

- Appel, K. W., Bash, J. O., Fahey, K. M., Foley, K. M., Gilliam, R. C., Hogrefe, C., Hutzell, W. T., Kang, D., Mathur, R., Murphy, B. N., Napelenok, S. L., Nolte, C. G., Pleim, J. E., Pouliot, G. A., Pye, H. O. T., Ran, L., Roselle, S. J., Sarwar, G., Schwede, D. B., Sidi, F. I., Spero, T. L., and Wong, D. C.: The Community Multiscale Air Quality (CMAQ) model versions 5.3 and 5.3.1: system updates and evaluation, *Geosci. Model Dev.*, 14, 2867-2897, 10.5194/gmd-14-2867-2021, 2021.
- Guenther, A. B., Jiang, X., Heald, C. L., Sakulyanontvittaya, T., Duhl, T., Emmons, L. K., and Wang, X.: The Model of Emissions of Gases and Aerosols from Nature version 2.1 (MEGAN2.1): an extended and updated framework for modeling biogenic emissions, *Geosci. Model Dev.*, 5, 1471-1492, 10.5194/gmd-5-1471-2012, 2012.
- Hu, J., Chen, J., Ying, Q., and Zhang, H.: One-year simulation of ozone and particulate matter in China using WRF/CMAQ modeling system, *Atmos. Chem. Phys.*, 16, 10333-10350, 10.5194/acp-16-10333-2016, 2016.
- Hua, J., Zhang, Y., de Foy, B., Shang, J., Schauer, J. J., Mei, X., Sulaymon, I. D., and Han, T.: Quantitative estimation of meteorological impacts and the COVID-19 lockdown reductions on NO₂ and PM_{2.5} over the Beijing area using Generalized Additive Models (GAM), *Journal of environmental management*, 291, 112676, 10.1016/j.jenvman.2021.112676, 2021.
- Mao, J., Li, L., Li, J., Sulaymon, I. D., Xiong, K., Wang, K., Zhu, J., Chen, G., Ye, F., Zhang, N., Qin, Y., Qin, M., and Hu, J.: Evaluation of Long-Term Modeling Fine Particulate Matter and Ozone in China During 2013–2019, *Frontiers in Environmental Science*, 10, 10.3389/fenvs.2022.872249, 2022.
- Sulaymon, I. D., Zhang, Y., Hopke, P. K., Zhang, Y., Hua, J., and Mei, X.: COVID-19 pandemic in Wuhan: Ambient air quality and the relationships between criteria air pollutants and meteorological variables before, during, and after lockdown, *Atmospheric research*, 250, 105362, 10.1016/j.atmosres.2020.105362, 2021a.
- Sulaymon, I. D., Zhang, Y., Hopke, P. K., Hu, J., Rupakheti, D., Xie, X., Zhang, Y., Ajibade, F. O., Hua, J., and She, Y.: Influence of transboundary air pollution and meteorology on air quality in three major cities of Anhui Province, China, *Journal of Cleaner Production*, 329, 129641, <https://doi.org/10.1016/j.jclepro.2021.129641>, 2021b.
- Wang, X., Li, L., Gong, K., Mao, J., Hu, J., Li, J., Liu, Z., Liao, H., Qiu, W., Yu, Y., Dong, H., Guo, S., Hu, M., Zeng, L., and Zhang, Y.: Modelling air quality during the EXPLORE-YRD campaign – Part I. Model performance evaluation and impacts of meteorological inputs and grid resolutions, *Atmospheric Environment*, 246, 118131, <https://doi.org/10.1016/j.atmosenv.2020.118131>, 2021.
- Wiedinmyer, C., Akagi, S. K., Yokelson, R. J., Emmons, L. K., Al-Saadi, J. A., Orlando, J. J., and Soja, A. J.: The Fire INventory from NCAR (FINN): a high resolution global model to estimate the emissions from open burning, *Geosci. Model Dev.*, 4, 625-641, 10.5194/gmd-4-625-2011, 2011.